

See discussions, stats, and author profiles for this publication at: <https://www.researchgate.net/publication/230900709>

Controlled Synthesis, Structural Evolution, and Photoluminescence Properties of Nanoscale One-Dimensional Hierarchical ZnO/ZnS Heterostructures

ARTICLE *in* THE JOURNAL OF PHYSICAL CHEMISTRY C · FEBRUARY 2011

Impact Factor: 4.77 · DOI: 10.1021/jp112047f

CITATIONS

24

READS

83

3 AUTHORS, INCLUDING:



Mashkoor Ahmad

Pakistan Atomic Energy Commission

47 PUBLICATIONS 934 CITATIONS

[SEE PROFILE](#)



Xingxu Yan

Tsinghua University

6 PUBLICATIONS 54 CITATIONS

[SEE PROFILE](#)

Controlled Synthesis, Structural Evolution, and Photoluminescence Properties of Nanoscale One-Dimensional Hierarchical ZnO/ZnS Heterostructures

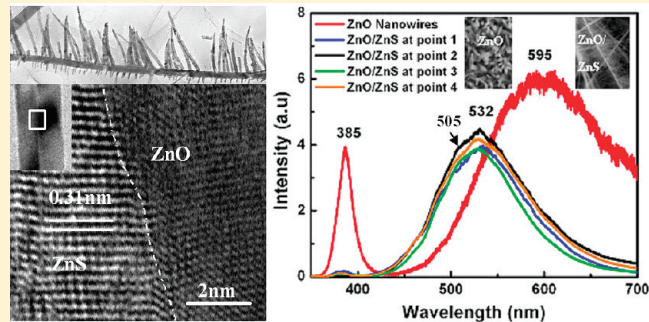
Mashkoor Ahmad,^{†,‡} Xingxu Yan,[†] and Jing Zhu^{*,†}

[†]Beijing National Center for Electron Microscopy, The State Key Laboratory of New Ceramics and Fine Processing, Laboratory of Advanced Material, China Iron & Steel Research Institute Group, Department of Material Science and Engineering, Tsinghua University, Beijing 100084, China

[‡]Physics Division, PINSTECH, Islamabad, Pakistan

 Supporting Information

ABSTRACT: One-dimensional (1-D) hierarchical heterostructures have attracted much attention due to potential applications in nanoscale building blocks for future optoelectronics devices and systems. In the present article, ZnO/ZnS heterostructures have been synthesized by a controlled vapor deposition method in which all the precursors are mixed together in the reaction chamber. The temperature, as well as the flow rate of the inert carrier Ar gas, plays an important role in defining the morphology of the heterostructures. The morphology and structure of as grown heterostructures have been characterized by field emission scanning electron microscopy, transmission electron microscopy, energy dispersive spectroscopy, X-ray diffraction, and X-ray photoelectron spectroscopy. The microscopic results reveal that the products consist of heterostructures with a variety of morphology. The structural analysis shows that the brushlike heterostructures are composed of side-by-side and up and down interfaces between two materials. In addition, the photoluminescence spectra of the heterostructures exhibit a strong blue-shift ~ 63 nm and an increase intensity of green emission which give them potential for optoelectronics devices. Furthermore, a brief growth mechanism has also been proposed.



1. INTRODUCTION

One-dimensional (1-D) nanostructures have attracted wide attention for their potential applications as building blocks for nanoscale devices. Various types of functional complex nanostructures with controlled structural characteristics (including morphology, dimensionality, surface architectures, and crystal structures) represent a significant challenge in the field of nanometer-scale science and technology. Intensive efforts have been devoted to achieve desired morphology or shape (such as cones, spheres, tubes, wires, belts, cables, brush, and branched heterostructures) and crystallinity of various inorganic crystals from micrometer to nanometer size. Among different nanostructures, 1-D heterostructures have become of particular interest with respect to potential applications in nanoscale heterostructured electronic devices, micro/nanoelectromechanical systems, optoelectronics, field emitters, light-emitting diodes^{1–12} and providing enhanced properties superior to a single system.^{13,14} For example, ZnO/ZnS heterojunctions make it possible to tailor the optical properties of nanostructures. These advantages make heterostructures one of the most promising candidates for the exploration of new applications. Furthermore, 1-D heterostructures can be classified into three types on the basis of the nature of the junctions, namely, segmented, coaxial core/shell, and hierarchical

heterostructures.¹⁵ Up until now different methods have been developed for the synthesis of 1-D heterostructures, such as template-directed methods, electrospinning, solution-phase method, lithography, electrodeposition, and vapor phase methods.^{16–20}

On the other hand, ZnO with band gap ~ 3.37 eV and ZnS with band gap ~ 3.68 eV at 300 K are important group II–VI semiconductors, and attract intense interest owing to their wide range of applications in optoelectronics, flat-panel displays, sensors, lasers, photovoltaic, electricity generation, and photocatalysis.^{21–25} Extensive effort has focused on the synthesis of ZnS and ZnO heterostructures such as ZnO/ZnS heterojunction nanoribbons, ZnO/ZnS nanobelts and nanowire heterostructures, and ZnO/ZnS coaxial cables.^{26–28,15} Here, we report for the first time the synthesis of a variety of 1-D heterostructures of ZnS and ZnO without any catalyst by a controlled thermal evaporation method.

2. EXPERIMENTAL SECTION

The synthesis of ZnS/ZnO heterostructures was carried out in a vacuum tube furnace, where the temperature, pressure, and

Received: November 26, 2010

Revised: December 22, 2010

Published: January 18, 2011

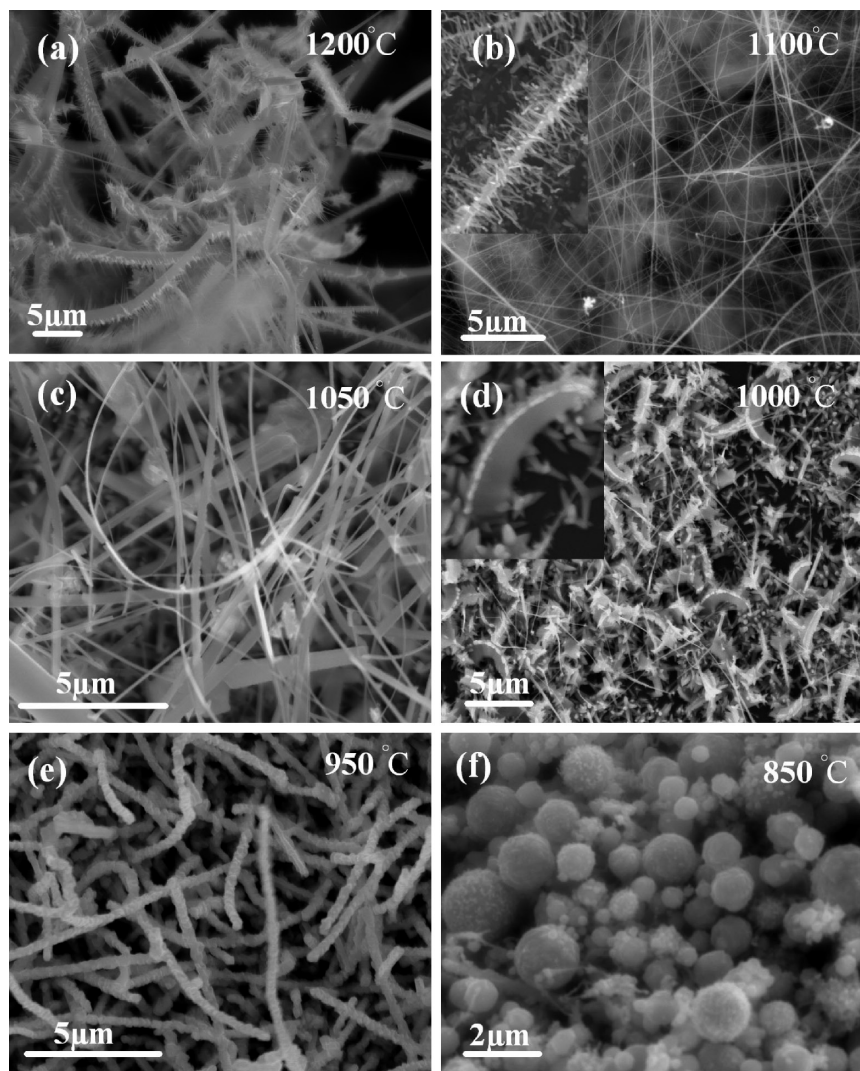


Figure 1. Field emission scanning electron microscopy images of synthesized ZnO/ZnS at different temperatures: (a) sawlike ultralong heterojunctions, (b) brushlike heterostructures (inset is the magnified image), (c) nanoribbons and nanobelts, (d) dendritelike heterostructure (inset is the magnified image), (e) snakelike heterostructures, and (f) microspheres.

flow rates of working gases are well-controlled. A quartz tube with an outer diameter of 30 mm and a length of 1200 mm was placed in a fixed alumina tube in a furnace. A mixture of 1 g of ZnS and 1 g of Zn powder (Alfa Aldrich, 99.9%) was placed at the center of the tube. Si wafers were placed at the downstream of the tube at about 20 cm away from the source. The tube was sealed and evacuated to a pressure of (133.32 Pa). The furnace was then heated to the desired temperatures at a rate of $20\text{ }^{\circ}\text{C min}^{-1}$ and kept at this temperature for 3 h. A constant flow of high-purity Ar was fed into the tube at a flow rate of 180 sccm throughout the entire heating and cooling processes. Highly pure O₂ was continuously fed into the tube at a flow rate of 1.5 sccm when the furnace temperature was at the desired temperature. After the furnace was naturally cooled to room temperature, the yellowish products deposited on the silicon wafers were collected and characterized using X-ray diffraction (XRD), scanning electron microscopy (SEM), energy dispersive spectroscopy (EDS), high-resolution tunnelling electron microscopy (HRTEM), X-ray photoelectron spectroscopy (XPS), and photoluminescence (PL).

3. RESULTS AND DISCUSSIONS

3.1. Morphology of the ZnO/ZnS Heterostructures. The morphology of the ZnO/ZnS heterostructures is investigated through SEM and found to be highly influenced by the experimental parameters such as temperature and flow rate of Ar gas. Heterostructures were synthesized at six different temperatures (850, 950, 1000, 1050, 1100, and 1200 °C) with fixed flow rate (180 sccm) as well as with two different flow rates (150 and 200 sccm). The product obtained at 1200 °C mainly consists of high-density ultralong heterostructures in the form of sawlike morphology, straight or curved as clearly seen from the SEM image in Figure 1a. The side view clearly shows that the whole sawlike nanostructure has a rectangular cross section, indicating the formation of sawlike structures. From close observation, it can be seen that at this typical temperature heterojunctions with diameter of ~200 nm and length ranging from several tens to hundreds of micrometers are achieved. Figure 1b is a low-magnification SEM image of the brushlike heterostructures obtained at 1100 °C and shows that the synthesized product

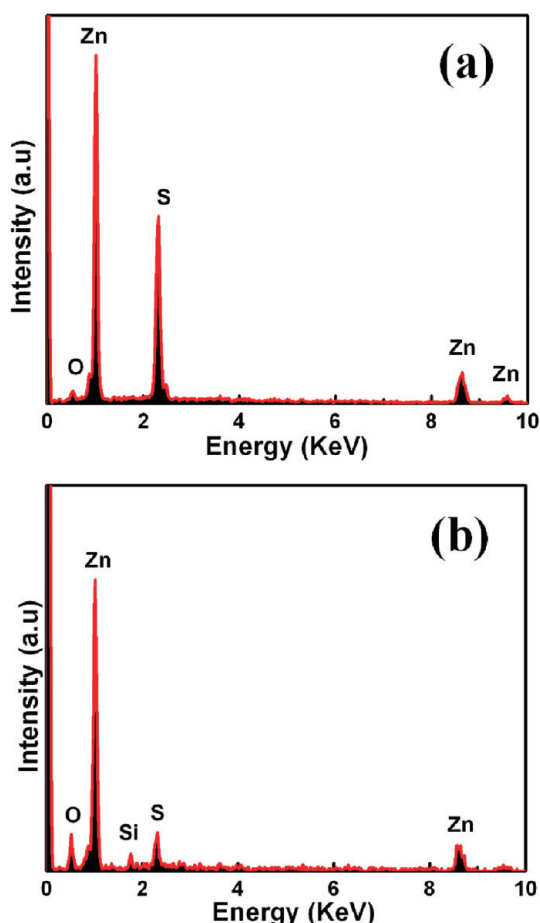


Figure 2. EDS spectra corresponding to (a) ultralong sawlike heterojunctions and (b) brushlike heterostructures.

mainly consists of a large number of micrometer-sized brushlike branched architectures. The inset in Figure 1b shows the close view of magnified SEM image of brushlike heterostructures and reveals that branches with a length of 2–3 and 3–5 μm are decorated around the trunk to form the architecture. These branches are oriented at an angle of 30°, 60°, and 90° with respect to their trunk. Figure 1c shows the SEM image of the product obtained at 1050 °C and reveals the formation of nanoribbons and nanobelts. The thickness of the nanobelts and nanoribbons is in the range of 100–200 nm and their length about tens to a hundred of micrometers. The formation of a large quantity of dendritelike heterostructures along with a small quantity of tetrapods is obtained at 1000 °C, as shown in Figure 1d. The dendritelike morphology with a little curve is clearly seen from the high magnification SEM image display in the inset. The side view clearly shows the uniform distribution of small teeth at one side. On the other hand, a snakelike heterostructures have been found at 950 °C, as shown in Figure 1e. The surface of snakelike heterostructures looks to be a little rough due to the influence of sulfur particles. At the same temperature, if the flow rate of Ar gas is increased or decreased, the snakelike heterostructure morphology changed to nanotubes and nanoribbons, respectively (Supporting Information). This shows that not only the temperature but also the flow gas has a strong effect on the morphology of the heterostructures. When the temperature is decreased at 850 °C, a change of morphology is observed.

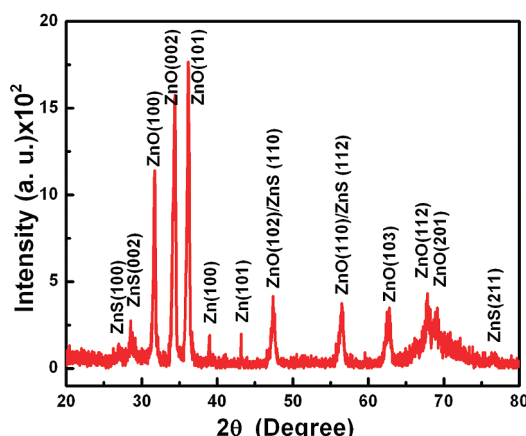


Figure 3. XRD pattern of ZnO/ZnS sample synthesized at 1100 °C.

In this case, instead of nanowire-like morphology, ZnO/ZnS microspheres are formed, as illustrated in Figure 1f. The diameter of these microspheres varies within 1–3 μm .

3.2. Structural and Compositional Analysis. The chemical composition of the ZnO/ZnS heterostructures is investigated through EDS. Figure 2a,b shows the EDS spectra of the heterostructures produced at 1200 and 1100 °C, revealing the chemical purity of the heterostructures. Similar observations are noticed from the EDS spectrum recorded for all other samples. The EDS spectra from these samples (not shown here) also consist of Zn, O, and S peaks, which confirm the presence of S in the product. The Si peak originated from the uncovered Si wafer.

The structure of the as-prepared product obtained at 1100 °C is also characterized using XRD. Figure 3 shows the XRD pattern of the brushlike heterostructures, in which all the peaks can be well-assigned to those of wurtzite (hexagonal) ZnS, with lattice constants of $a = 0.382 \text{ nm}$ and $c = 0.626 \text{ nm}$ (JCPDS: 36-1450), and wurtzite (hexagonal) ZnO, with lattice constants of $a = 0.325 \text{ nm}$ and $c = 0.521 \text{ nm}$ (JCPDS: 36-1451). The existence of Zn peaks in the pattern reveals that a small amount of Zn powder remains phase-separated during the experiment. Similar XRD spectra are also observed from all other samples (not shown here).

The detailed microstructure and composition of the brushlike heterostructures is characterized using transmission electron microscopy (TEM). Figure 4a is a low-magnification TEM image taken from a section of a typical ZnO/ZnS architecture obtained at 1100 °C and shows that the architecture has an array of the oriented nonuniform distribution of branched nanowires (NWs) grown around the trunk. We can clearly see that one side of the trunk is composed of small-branch NWs oriented at 90° with typical length in the range of 2–3 μm . A clear observation suggests that these 1-D heterostructures are composed of the same material from the trunk and the branch NWs. It can be clearly seen that each branch NW has a conelike structure. From the statistic analysis of over 20 branch NWs, the tip and bottom diameters of these cone-shaped NWs are in the range of 5–10 and 50–200 nm, respectively, which is consistent with the SEM observations. Figure 4b is a high-magnification TEM image of a single-branch NW which clearly displays the ZnO and ZnS side-by-side structure of different contrast. The in situ EDS elemental analysis in Figure 4c,d, taken from the area indicated with a circle and rectangle in Figure 4b, shows that each branch NW in the brushlike heterostructure contains only Zn, O, and S.

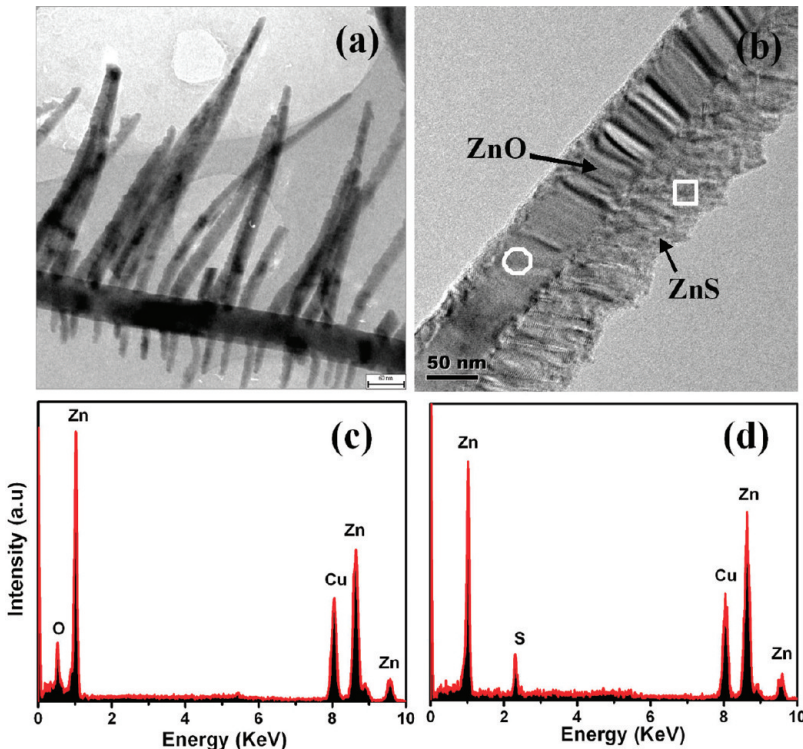


Figure 4. (a) Low-magnification TEM images of brushlike heterostructures, (b) magnified image of a single-branch NW oriented at 60° , and EDS spectrum of (c) ZnO section and (d) ZnS section.

side-by-side, respectively. The Cu signal comes from the surface of the copper grid used for TEM measurements.

Figure 5a is a high-resolution TEM image taken from the long-branch NW of the brushlike heterostructure oriented at 60° and clearly displays the wurtzite ZnO and ZnS side-by-side structure of different contrast. Figure 5b shows the HRTEM image taken from the indicated area of a single small-branch NW oriented at 90° . The detailed structural analysis shows that the entire small-branch NW is composed of a segmented up and down interface of ZnO and ZnS. The lattice fringes are measured to be 0.261 nm at the top part and 0.31 nm at the bottom part, which correspond to the wurtzite ZnO and ZnS, respectively. This observation clearly shows the up and down interface between two materials. Figure 5c–e shows the HRTEM images taken from different branch NWs oriented at 30° and 60° in order to confirm the structures. It can be clearly seen from Figure 5c–e that the entire branched NWs are composed of ZnO/ZnS heterostructure with side-by-side interfaces. In order to further investigate the structures of branch NWs, HRTEM measurements on more than 20 different branch NWs have also been performed to ensure reproducibility.

The purity and composition of the brushlike heterostructure has been analyzed by XPS analysis. Figure 6a shows the XPS survey spectrum in which S, Zn, O, and C peaks can be clearly observed. In Figure 6b, the peak at binding energy 530.4 and 531.7 eV are ascribed to lattice oxygen in the ZnO/ZnS structure. The spectrum in Figure 6c shows that the peaks at the binding energies of 161.6 and 162.5 eV could be assigned to $S2p_{3/2}$ and $S2p_{1/2}$ in the Zn–S bond, respectively.²⁹ The $S2p$ peak in the spectrum clearly indicates the existence of S element in heterostructures. On the other hand, the XPS spectrum of Zn is also shown in Figure 6d corresponding to $Zn2p_{3/2}$ and $Zn2p_{1/2}$ peaks

located at the binding energies of 1020.8 and 1043.2 eV, respectively. These XPS results are also in good agreement with the previous reports.^{30–32} Therefore, XPS analysis again confirms the deposition of ZnO/ZnS heterostructure on the substrate.

3.3. Photoluminescence Property. Figure 7a shows the room temperature PL spectra of ZnO NWs and ZnO/ZnS brushlike heterostructure. For comparison, ZnO NWs were synthesized by the same vapor deposition method under the same conditions. The spectrum of ZnO NWs consists of a UV peak at 385 nm and a strong broad green emission at ~ 475 – 700 nm centered at ~ 595 nm. In comparison, the ZnO/ZnS brushlike heterostructure exhibits a weak UV emission at ~ 382 nm and a wide green emission band at ~ 430 – 630 nm centered at ~ 532 nm. The green emission in the present experiment is mainly originating from some self-activated centers, such as the singly ionized charge state of specific defects, oxygen vacancies, and elemental sulfur atoms vacancy resulting from the lattice mismatch between ZnS and ZnO at the interface region.^{33–35} It can be seen that besides green emission peak, a small shoulder peak at ~ 505 nm is also observed for the heterostructures that could be assigned to the presence of ZnO/ZnS interface, as reported.³⁶ In contrast to ZnO, the depression and green emission peak position has a blue-shift of about ~ 63 nm. This blue-shift is due to the sulfur incorporation and ZnO/ZnS interfaces in the heterostructures, which is consistent with the previous report.³⁷ The decrease in the intensity of UV emission could be attributed to the increased amount of lattice interstitials defects, such as interstitial S atoms and the nature of the surface stats, as reported.³⁸

A more detailed mechanism of the origination of the green emission in the synthesized ZnO/ZnS heterostructures is also studied. In this study, the influence of growth temperature on the

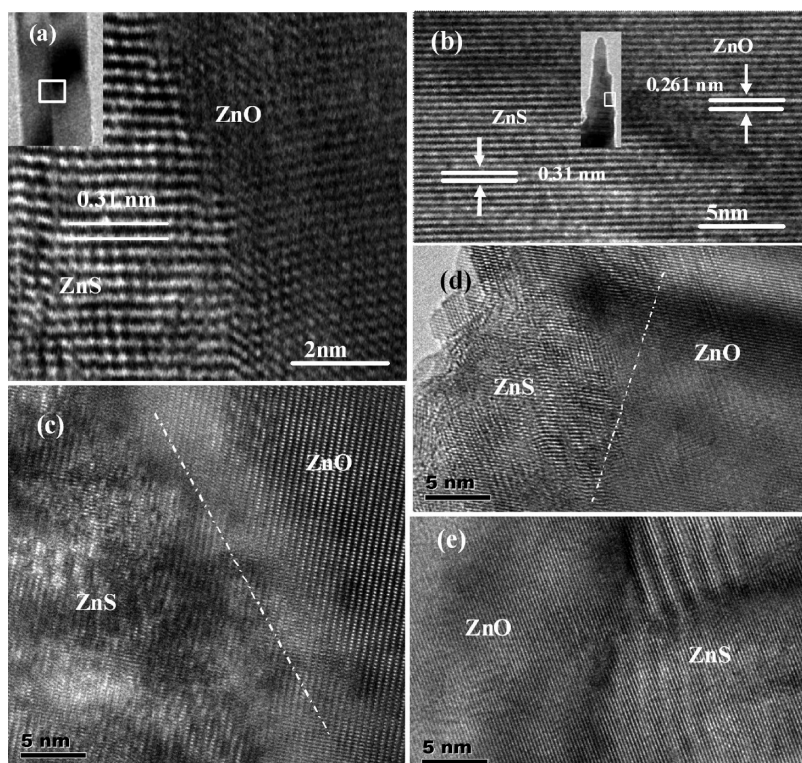


Figure 5. HRTEM images of (a) brushlike heterostructures with branch NWs around the trunk (inset is the corresponding TEM image), (b) ZnO/ZnS up and down interface section of the small individual branch NW as shown in the inset, (c, d) HRTEM images from three different branch NWs oriented at 30° and 60° that display clear interface between two materials.

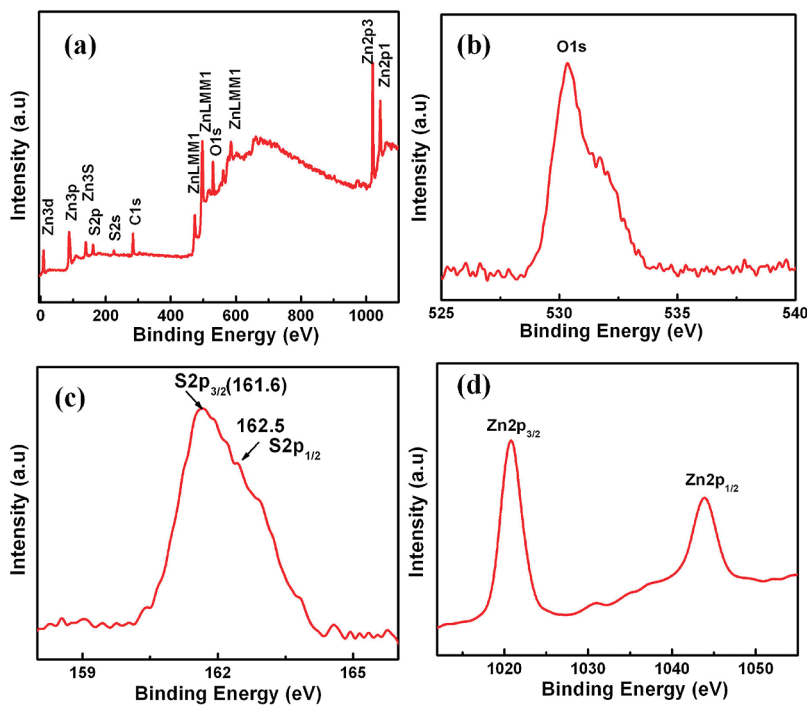


Figure 6. XPS spectra of ZnO/ZnS brushlike heterostructures: (a) complete survey and (b) O1s, (c) S2p, and (d) Zn2p peaks.

optical properties of the heterostructures is investigated by PL. Figure 7b shows the PL performance of the heterostructures synthesized at different temperatures. It has been found that growth temperature has a direct correlation with the intensity of

green emission in the heterostructures. It can be seen that the increase in growth temperature significantly increased the intensity of green emission as well as a small shift in peaks, which is considered due to the difference in morphology, the density of

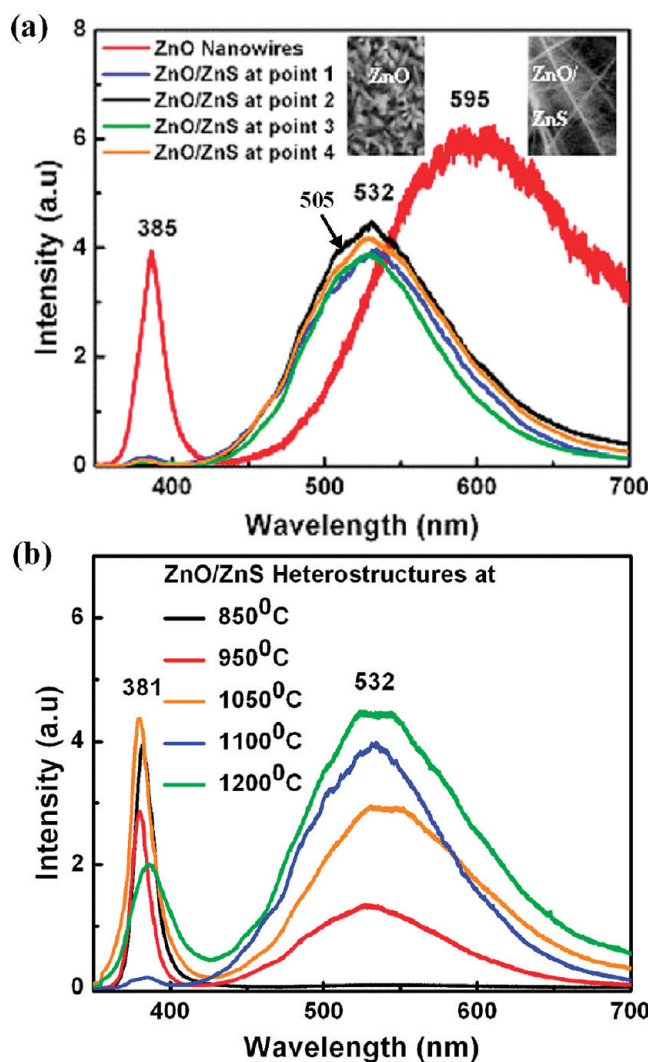


Figure 7. Room temperature PL spectra of (a) ZnO NWs and ZnO/ZnS brushlike heterostructures taken from different points and (b) ZnO/ZnS heterostructures synthesized at different temperatures.

native defects induced in the structures, such as incorporation of more sulfur atoms, and the nature of interfaces, as reported in the literature. On the basis of the EDS spectra in Figure 2a, the presence of excessive S is also correlated with the intensity of the green emission.

3.4. Growth Mechanism. The growth mechanism of the present heterostructures is not fully understood; therefore, a preliminary growth model is proposed here. On the basis of the SEM and HRTEM image observations, no nanoparticles were observed at the ends of the nanowires, suggesting that the growth of these ZnO/ZnS heterostructures should not be explained by the common vapor–liquid–solid growth mechanism.³⁹ Therefore, the growth of the ZnS/ZnO heterostructures appears to follow the vapor–solid mechanism and to proceed as follows. As the furnace temperature reached 500 °C, the Zn powder evaporates and is carried in the flow of Ar and deposited at the Si substrates. These deposited Zn particles acts as the nucleation for the growth of ZnO/ZnS hierarchical heterostructures. When the furnace was heated to desired temperature, ZnS powder would first evaporate and decompose to Zn and S vapors. The Zn and S vapors would then be carried by the mixture gas (Ar flow at

Table 1. Growth Evolution of ZnO/ZnS Heterostructures at Different Experimental Conditions^a

| source Zn:ZnS | Ar flow (sccm) | temperature (°C) | time (h) | morphology |
|------------------|-------------------|---------------------|-------------|-----------------------------------|
| 1:1 | 180 | 1200 | 3 | ultralong sawlike heterojunctions |
| 1:1 | 180 | 1100 | 3 | brushlike heterostructures |
| 1:1 | 180 | 1050 | 3 | nanoribbons and nanobelts |
| 1:1 | 180 | 1000 | 3 | dendritelike heterostructures |
| 1:1 | 180 | 900 | 3 | snakelike heterostructures |
| 1:1 | 180 | 850 | 3 | ZnS/ZnO microspheres |
| 1:1 | 150 | 950 | 2 | nanoribbon-like heterostructures |
| 1:1 | 200 | 950 | 2 | ZnS/ZnO nanotubes |

^a Oxygen flow rate throughout in this work remains at 1.5 sccm.

a rate of 180 sccm and O₂ flow at 1.5 sccm) and travel to the low-temperature region of the furnace tube, where they would be absorbed into the Zn droplets on the silicon wafer. O₂ would also be absorbed into the Zn droplet and react with the solubilized Zn to form ZnO, due to the greater formation enthalpy of ZnO than that of ZnS under the same conditions. When the concentrations of ZnS and ZnO in the droplets have reached supersaturation at the substrate temperature, ZnS and ZnO crystals would precipitate and then start to form the heterostructures.

The growth and structural evolution of the ZnO/ZnS heterostructures formation at different experimental conditions are summarized in Table 1. It is confirmed that not only the temperature but also the flow rate of the Ar gas are crucial parameters in defining the morphology of the heterostructures.

4. CONCLUSIONS

In summary, rapid, large-scale production of ZnS/ZnO heterostructures has been achieved on Si substrate without any catalyst by controlled thermal evaporation. Morphology of the heterostructures is controlled by varying the temperature, as well as the flow rate of the Ar gas. It has been found that brushlike heterostructures are composed of branch ZnS/ZnO NWs with side-by-side and up and down interfaces between two materials. Furthermore, PL spectra of the heterostructures exhibit a strong blue-shift ~63 nm at room temperature. It has been found that an increase in growth temperature enhances the green emission intensity due to the sulfur incorporation and the formation of ZnO/ZnS interfaces. In addition, it has been found that Zn also plays an important role in the growth of heterostructures. We suggest that this method can be utilized to synthesize a variety of heterostructures at the nanoscale. These heterostructures may provide unique applications such as field emitters and in photocatalysis and optoelectronic devices for surgery and spectroscopy.

■ ASSOCIATED CONTENT

S Supporting Information. ZnO/ZnS heterostructures synthesized at different Ar flow rates. This material is available free of charge via the Internet at <http://pubs.acs.org>.

■ AUTHOR INFORMATION

Corresponding Author

*E-mail: Jzhu@mail.tsinghua.edu.cn. Fax: 86-10-62771160.

■ ACKNOWLEDGMENT

This work is financially supported by National 973 Project of China and Chinese National Nature Science Foundation. This work made use of the resources of the Beijing National Center for Electron Microscopy. The authors are also grateful to the Higher Education Commission (HEC) Pakistan for the financial support to Mashkoor Ahmad.

■ REFERENCES

- (1) Gudiksen, M. S.; Lauhon, L. J.; Wang, J.; Smith, D. C.; Lieber, C. M. *Nature* **2002**, *415*, 617.
- (2) Verheijen, M. A.; Immink, G.; De Smet, T.; Borgstrom, M. T.; Bakkers, E. P. A. M. *J. Am. Chem. Soc.* **2006**, *128*, 1353.
- (3) Dick, K. A.; Deppert, K.; Larsson, M. W.; Martensson, T.; Seifert, W.; Wallenberg, L. R.; Samuelson, L. *Nat. Mater.* **2004**, *3*, 380.
- (4) Wang, C. R.; Wang, J.; Li, Q.; Yi, G. C. *Adv. Funct. Mater.* **2005**, *15*, 1471.
- (5) Han, S.; Li, C.; Liu, Z.; Lei, B.; Zhang, D.; Jin, W.; Liu, X.; Tang, T.; Zhou, C. W. *Nano Lett.* **2004**, *4*, 1241.
- (6) Yin, L. W.; Bando, Y.; Zhu, Y. C.; Li, M. S.; Li, Y. B.; Golberg, D. *Adv. Mater.* **2005**, *17*, 110.
- (7) Wang, Z. L.; Song, J. H. *Science* **2006**, *312*, 242.
- (8) Watt, J.; Young, N.; Haigh, S.; Kirkland, A.; Tilley, R. D. *Adv. Mater.* **2009**, *21*, 2288.
- (9) Chen, Z. G.; Zou, J.; Wang, D. W.; Yin, L. C.; Liu, G.; Sun, C. H.; Liu, Q. F.; Yao, X. D.; Li, F.; Yuan, X. L.; Sekiguchi, T.; Lu, G. Q.; Cheng, H. M. *Adv. Funct. Mater.* **2009**, *19*, 484.
- (10) Luo, J.; Zhang, L.; Zhu, J. *Adv. Mater.* **2003**, *15*, 579.
- (11) Luo, J.; Huang, Z.; Zhao, Y.; Zhang, L.; Zhu, J. *Adv. Mater.* **2004**, *16*, 1215.
- (12) Luo, J.; Xing, Y.; Zhu, J.; Yu, D.; Zhao, Y.; Zhang, L.; Fang, H.; Huang, Z.; Lu, J. *Adv. Funct. Mater.* **2006**, *16*, 1081.
- (13) Lauhon, L. J.; Gudiksen, M. S.; Wang, D. L.; Lieber, C. M. *Nature* **2002**, *420*, 57.
- (14) Wu, Y.; Xiang, J.; Yang, C.; Lu, W.; Lieber, C. M. *Nature* **2004**, *430*, 61.
- (15) Shen, G. Z.; Chen, D.; Bando, Y.; Golberg, D. *J. Mater. Sci. Technol.* **2008**, *24*, 541.
- (16) Xia, Y. N.; Yang, P. D.; Sun, Y.; Wu, Y.; Mayers, B.; Gates, B.; Yin, Y.; Kim, F.; Yan, H. *Adv. Mater.* **2003**, *15*, 353.
- (17) Shen, G. Z.; Chen, D. *J. Am. Chem. Soc.* **2006**, *128*, 11762.
- (18) Dai, H. *Acc. Chem. Res.* **2002**, *35*, 1035.
- (19) Pan, Z. W.; Dai, Z. R.; Wang, Z. L. *Science* **2001**, *291*, 1947.
- (20) Shen, G. Z.; Bando, Y.; Hu, J. Q.; Golberg, D. *Appl. Phys. Lett.* **2007**, *90*, 123101.
- (21) Fang, X. S.; Zhang, L. D. *J. Mater. Sci. Technol.* **2006**, *22*, 721.
- (22) Moore, D.; Wang, Z. L. *J. Mater. Chem.* **2006**, *16*, 3898.
- (23) Fang, X.; Bando, Y.; Gautam, U. K.; Zhai, T.; Zeng, H.; Xu, X.; Liao, M.; Golberg, D. *Solid State Mater. Sci.* **2009**, *34*, 190.
- (24) Schrier, J.; Demchenko, D. O.; Wang, L. W. *Nano Lett.* **2007**, *7*, 2377.
- (25) Lu, M. Y.; Song, J.; Lu, M. P.; Lee, C. Y.; Chen, L. J.; Wang, Z. L. *ACS Nano* **2009**, *3*, 357.
- (26) Zapien, J. A.; Jiang, Y.; Meng, X. M.; Chen, W.; Au, F. C. K.; Lifshitz, Y.; Lee, S. T. *Appl. Phys. Lett.* **2004**, *84*, 1189.
- (27) Ju, S.; Facchetti, A.; Xuan, Y.; Liu, J.; Ishikawa, F.; Ye, P. D.; Zhou, C. W.; Marks, T. J.; Janes, D. B. *Nat. Nanotechnol.* **2007**, *2*, 378.
- (28) Fan, X.; Zhang, M. L.; Shafiq, I.; Zhang, W. J.; Lee, C. S.; Lee, S. T. *Adv. Mater.* **2009**, *21*, 2393.
- (29) Kim, D. P.; Kim, C. I.; Kwon, K. H. *Thin Solid Films* **2004**, *459*, 131.
- (30) Ahmad, M.; Zhu, J. *J. Mater. Chem.* **2011**, *21*, 599.
- (31) Ahmad, M.; Zhao, J.; Iqbal, J.; Miao, W.; Xie, L.; Mo, R.; Zhu, J. *J. Phys. D: Appl. Phys.* **2009**, *45*, 165406.
- (32) Ahmad, M.; Pan, C.; Iqbal, J.; Gan, L.; Zhu, J. *Chem. Phys. Lett.* **2009**, *480*, 105.
- (33) Yin, L. W.; Bando, Y.; Zhan, J. H.; Li, M. S.; Golberg, D. *Adv. Mater.* **2005**, *17*, 1972.
- (34) Ye, C. H.; Fang, X. S.; Wang, M.; Zhang, L. D. *J. Appl. Phys.* **2006**, *99*, 063504.
- (35) Zheng, H.; Duan, G.; Li, Y.; Yang, S.; Xu, X.; Cai, W. *Adv. Funct. Mater.* **2010**, *20*, 561.
- (36) Peng, H.; Liuyang, B.; Lingjie, Y.; Jinlin, L.; Fangli, Y.; Yunfa, C. *Nanoscale Res. Lett.* **2009**, *4*, 1047.
- (37) Zeng, H.; Cai, W.; Li, Y.; Hu, J.; Liu, P. *J. Phys. Chem. B* **2005**, *109*, 18265.
- (38) Shen, G. Z.; Chen, D.; Lee, J. C. *J. Phys. Chem. B* **2006**, *110*, 15689.
- (39) Morales, A. M.; Lieber, C. M. *Science* **1998**, *279*, 208.